





Investigation of Cobalt Substitution on the Structural, Optical Band Gap, and Photocatalytic Dye Degradation Properties of Spray Deposited SnO₂ Thin Films

Sadasivam Kumaravelan^{1,*} , Raghavan Sambasivam¹ , Poona Mohammed Mohammed Gazzali² , Syed Masood Fairose³ 

¹ Urumu Dhanalakshmi College (Affiliated to Bharathidasan University), Kattur 620019, Tamilnadu, India; skumaravelanphy@gmail.com (S.K.); sambasivam63@gmail.com (R.S.);

² Department of Materials Science, University of Madras, Chennai - 600025, Tamilnadu, India; drmgf.21@gmail.com (P.M.M.G.);

³ School of Optometry, Institute of Ophthalmology- Joseph Eye Hospital, Melapudur, Tiruchirapalli - 620001, Tamilnadu, India; fairose170489@gmail.com (S.F.);

* Correspondence: skumaravelanphy@gmail.com (S.K.);

Scopus Author ID 57219052226

Received: 30.05.2022; Accepted: 21.06.2022; Published: 11.09.2022

Abstract: Pure and cobalt substituted tin oxide thin films are successfully formed on a glass substrate using the simple spray pyrolysis technique. XRD patterns reveal the polycrystalline nature of the samples with tetragonal rutile structure. The shift in X-ray diffraction peak to a higher 2θ value and its subsequent contraction of the SnO₂ rutile lattice along the c-axis manifests the infusion of the guest cobalt ions. Crystallite size and microstrain values are found to vary with cobalt substitution. SEM analysis shows the uniform dispersion of the nanoparticles in the prepared thin films. The optical band gap values are found to narrow down with cobalt substitution from 4.04 eV–3.93 eV. Photoluminescence study hints at the presence of intermediate states within the forbidden energy band gap of SnO₂. Photocatalytic dye degradation of Methylene blue (MB) highlights the role of cobalt with a high photocatalytic activity of 86 % compared to other investigated thin films.

Keywords: spray; deposition technique; dye degradation; X-ray diffraction; semiconducting material; band gap.

© 2022 by the authors. This article is an open-access article distributed under the terms and conditions of the Creative Commons Attribution (CC BY) license (<https://creativecommons.org/licenses/by/4.0/>).

1. Introduction

Recently, water pollutants have posed a severe threat to human society in many forms. The precious elixir 'water' is accidentally polluted or manufactured for an industrial cause. Industrial effluents contain hazardous chemicals, which are released at an alarming rate with the skyrocketing hike in production. These chemicals/ effluents are released from oil refineries, livestock dips, sewage disposal, tanneries, and textile industries. Many of these pollutants have carcinogenic properties and hence mark an immediate and permanent threat to human society, livestock, the aquatic ecosystem, and the entire environment where we live. Photocatalysis, as the name suggests the catalysis uses photons of certain energy obtained either natural or artificial to degrade the harmful chemicals in the dye mixture, thus facilitating a promising solution for one major cause of water pollutants [1-4]. Fujishima and Honda utilized this interesting technique for dye-degradation in 1972, and the underlying process is the reaction between photochemistry and the solid material [5,6]. Confiscation of toxic organic and

inorganic pollutants, especially from water, with the aid of semiconductor photocatalysts, has been a topic of research since then, as they offer a platform for green technology [7-12].

Among various metal oxides, SnO₂, with the vast tuning of band gap 3.2 – 4.2 eV, n-type conductivity, and substitutional compatibility, find itself as a potential candidate for gas sensors, transparent conducting electrodes, solar cells, lithium-ion batteries applications, etc.[13-45]. SnO₂ thin films are suggested to play a crucial role in photocatalysis due to their multi-functional characteristics. However, for any fruitful SnO₂-based photocatalytic activity limited by quick electron-hole pair recombination, it is necessary to create an additional scattering mechanism via impurity doping especially transition metal ions.

Cobalt ions, on the other hand, are found to impede grain growth and hence play a crucial role in tuning the optical properties of SnO₂ [46-48]. Different shapes and structures of SnO₂ NPs have been attempted; round-shaped structures offer improved crystallinity and photocatalytic activity [49-54]. However, while using powders for the real-time dye degradation process, issues related to the catalyst may settle down and accumulate in our aquatic ecosystem. A few possible solutions to this issue may be recovering the catalyst via magnetic activity or even not letting them settle using a thin film photocatalyst. In the present work, Co-substituted SnO₂ thin films using spray pyrolysis are attempted. The spray pyrolysis method is advantageous by means of its simple and rapid synthesis and easy control of particle size and composition. The chosen Co-substituted SnO₂ thin film preparation process is ideal for photocatalysis as it magnifies the separation of photo-generated electron and hole pair. The Co ions in Co-substituted SnO₂ thin films can facilitate an electron efficiently from the conduction band of SnO₂ to an oxygen molecule in solution, rendering it a novel material for photocatalytic reaction.

2. Experimental details

2.1. Film preparation.

Pure and Co substituted (2-8%) SnO₂ thin film samples are prepared using cobalt acetate, stannous chloride, and hydrogen chloride as precursors. Thin films of SnO₂ and Co substituted SnO₂ coated on glass substrates following the reaction sequence as mentioned in Ref. [15].

2.2. Characterization.

The phase identification was carried out using PAN analytical X'Pert PRO-PW3040 diffractometer with Cu K α x-ray radiation ($\lambda = 1.5406 \text{ \AA}$). The optical property viz, absorbance/reflectance, and photoluminescence are studied using Jasco--570, UV-Vis-NIR Spectrophotometer, Japan, and Spectrofluorophotometer (Shimadzu RF-5301), respectively. Surface morphology is analyzed using Carl Zeiss, EVO 8 instrument.

2.3. Photocatalytic test.

The photocatalytic behavior of the pure and (2% to 8%) cobalt-substituted SnO₂ thin films is evaluated by the removal of Methylene blue dye (C₁₆H₁₈ClN₃S) under a UV light source. A Xe (Xenon) lamp is used as the light source, and the distance between the UV source and the photo-reaction vessel is kept at 10 cm. The suspensions are magnetically stirred in the dark for 30 min prior to irradiation. Then, the photoreaction vessel is exposed to UV irradiation

under standard ambient conditions. The selected dye concentration is used in conjunction with thin films (Area= 2.5*7.5 cm²) in the photocatalytic dye degradation experiment. At regular time intervals (0, 15, 30, 45, 60, 75, 90, and 105 minutes), 3 mL of the suspension is pipetted out for further evaluation using a UV-Vis absorption spectrometer. The photo-removal efficiency percentage is calculated from the equation given below:

$$\% \text{ Photo-removal efficiency} = (C_0 - C)/C_0 \times 100$$

where, C_0 is the initial concentration of dye and C is the concentration of dye after photo-irradiation for the selected time interval.

3. Results and Discussion

3.1. Structural properties.

The phase formation of the investigated Co: SnO₂ thin films were performed using a powder X-ray diffractometer, and the resulting 2θ vs. intensity profiles are shown in Figure 1.

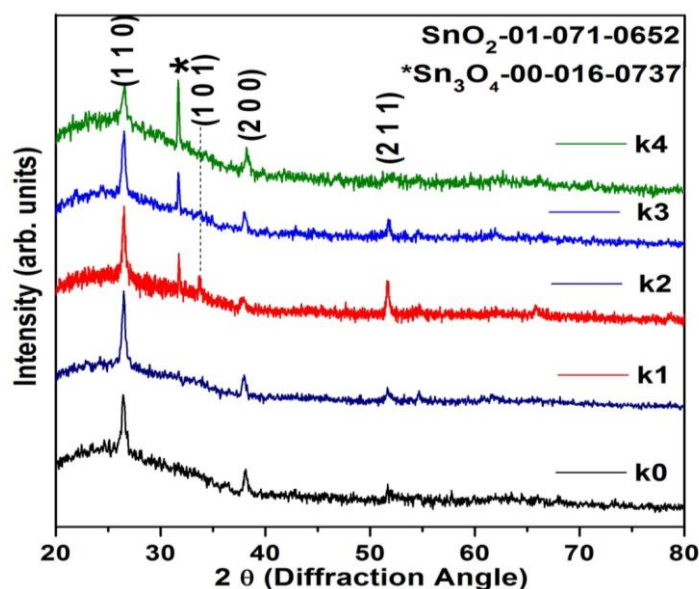


Figure 1. XRD patterns of undoped and Co-doped SnO₂ thin films.

Table 1. Lattice parameters, crystallite size, strain, and band gap energy values of Co substituted SnO₂ thin films samples.

Sample	Lattice parameter (Å)		c/a	Crystallite Size (D) (nm)	Strain (ε) x 10 ⁻³	Band gap (eV)
	(a)	(c)				
K0	4.7262	3.1839	0.6736	33	5.761	4.04
K1	4.7512	3.1744	0.6681	34	5.662	4.03
K2	4.7587	3.1708	0.6663	38	4.838	3.97
K3	4.7517	3.1586	0.6647	33	5.896	3.95
K4	4.7089	3.1396	0.6667	56	3.065	3.93

The XRD patterns show that the thin film samples exhibit tetragonal Rutile SnO₂ structure space group 136: P4₂/mmn, JCPDS 01-071-0652, along with some minor secondary phases upon increasing the Co concentrations. In addition, peaks correspond to Sn₃O₄ for 4%, 6%, and 8% of Co-substituted SnO₂ samples. The X-ray diffraction peaks shift reveals cobalt ions' incorporation into the SnO₂ lattice (Figure 2) [55]. The lattice parameters, crystallite size, and strain are calculated from the diffraction patterns, and the values are summarized in Table 1.

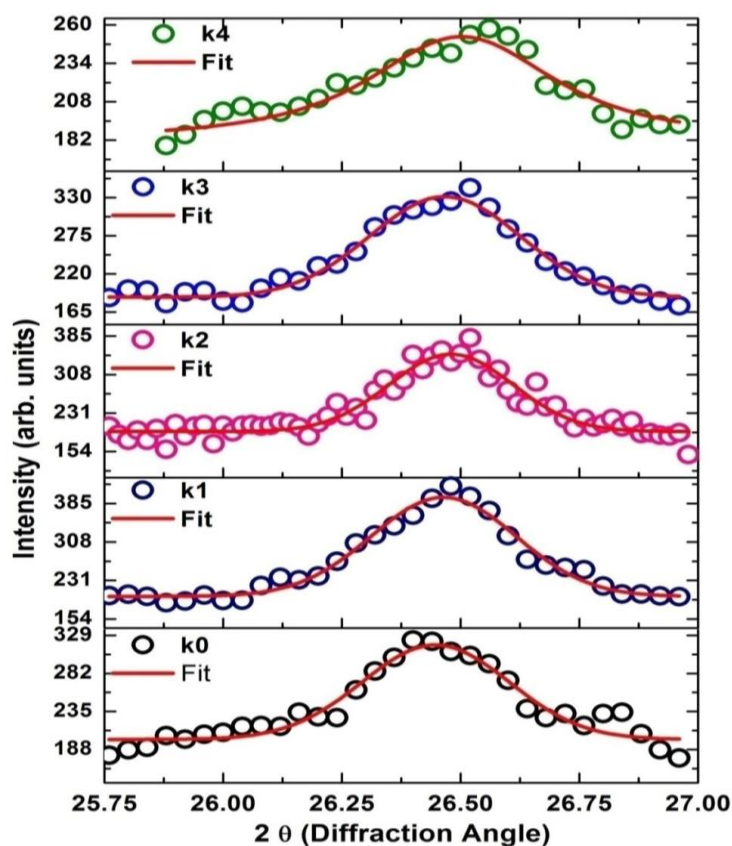


Figure 2. Variation in (1 1 0) peak position of SnO₂ thin films upon incorporating cobalt ions.

Interestingly, an expansion along the a-axis and contraction along the c-axis is observed with the doping of cobalt ions. The tetragonal distortion (c/a) decreases with increasing Co concentration. Further, there is a positive shift of (1 1 0) plane upon cobalt substitution, as shown in Figure 2. It may be attributed to the ionic radius size effect between Sn⁴⁺ and Co²⁺ ions. Further, crystallite size and crystallinity are also found to increase with Co substitution. The lattice of SnO₂ is found to relax upon infusion of cobalt ions which is realized by the reduction in microstrain values [56]. The full width at half maxima (β) and lattice strain (ϵ) are related to each other as $\epsilon = \beta \cos \theta / 4$ [57]. According to the Scherrer equation, the crystallite size (D) and β were inversely related. Thus, strain is found to decrease with increasing crystallite size—the pristine SnO₂ exhibits maximum lattice with the least crystallite size value among the investigated thin film samples.

3.2. Optical properties.

There is a discrepancy in the band gap values for the investigated SnO₂ sample. It is given in below three graphs 3, 4, and 5.

Figure 3 shows the band gap of selected literature sources [13,15-40,58]. In the present work, pristine SnO₂ thin films exhibit the maximum value optical band gap (E_g) as 4.04 eV, which agrees with the literature values [59]. The varying band gap values from 3.2 to 4.2 eV for the pure SnO₂ sample are given in Figure 3.

E_g of SnO₂ compounds are found to vary with calcination temperature, as shown in Figure 4. Band gap values of the SnO₂ compounds increase with the increase in the calcination temperature, which can be attributed to crystallite size, crystallinity, and defect associated with oxygen vacancies [58]. Similarly, According to the increase in the calcination temperature, the band gap decreased sharply due to the sinterization or segregation of SnO₂ particles [60].

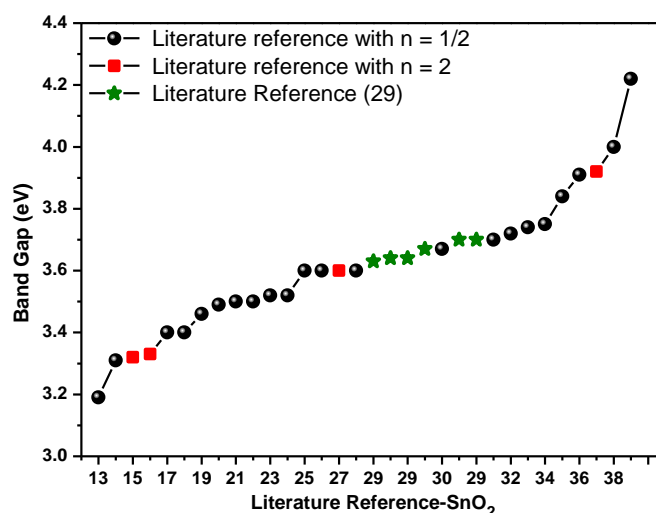


Figure 3. Band gap values of pure SnO₂ samples from selected literature. Black solid sphere refers to band gap values calculated with exponent factor (n) value of $1/2$. Red solid square refers to band gap values calculated with exponent factor (n) value of 2. Green solid stars refer to the same literature source with different band gap values for different calcination temperatures. Numbers given on the x-axis denote the respective literature reference number.

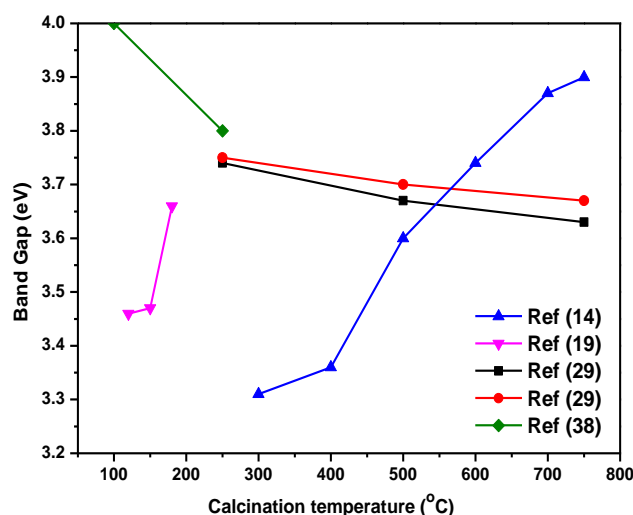


Figure 4. Variation of the band gap of SnO₂ compounds with calcination temperature from selected literature. Numbers in the parenthesis refer to the respective literature.

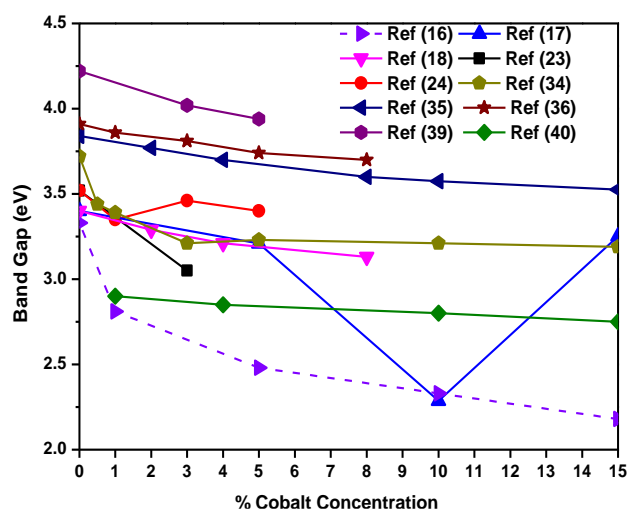


Figure 5. Band gap values of Co substituted SnO₂ compounds from selected literature. Numbers in the parenthesis refer to the respective literature.

The band gap values of Co substituted SnO₂ compounds given in Figure 5, is found to decrease with increasing the doping concentration, which may be attributed to several reasons, among them prominent ones, band bending occurs around the edges, charge transfer between cobalt and tin ions and the alloying effect [61-63]. From the literature, the band gap of the SnO₂ compounds depends on the preparation techniques, calcination temperature, size, morphology, and doping.

3.2.1. Diffused Reflectance Spectra.

The optical properties of the prepared Co:SnO₂ thin films have been studied by calculating the band gap. The optical band gap is estimated by using a modified Kubelka-Munk (K-M) formula, as given below [64]:

$$F(R)=\alpha/S=(1-R)^2/2R$$

where $F(R)$, α , S , and R are the K-M function, absorption coefficient, scattering factor, and sample reflectance, respectively.

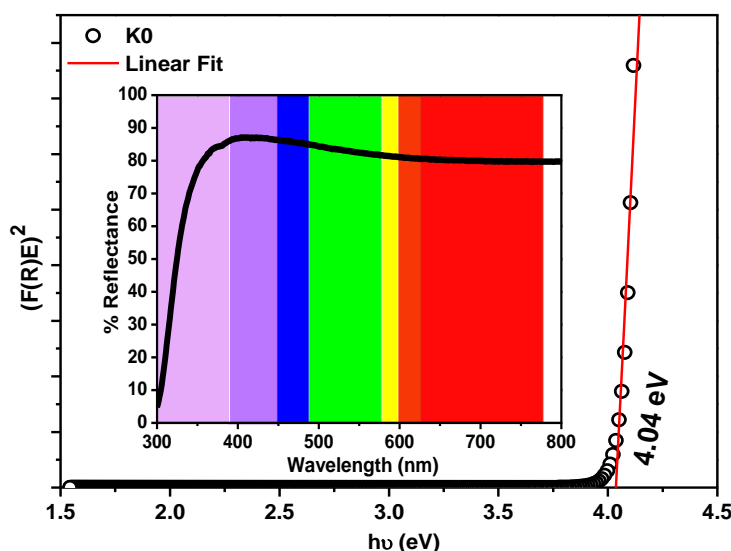


Figure 6. Modified Kubelka-Munk plot of pure SnO₂ thin films. The inset shows the reflectance spectrum of SnO₂ thin films.

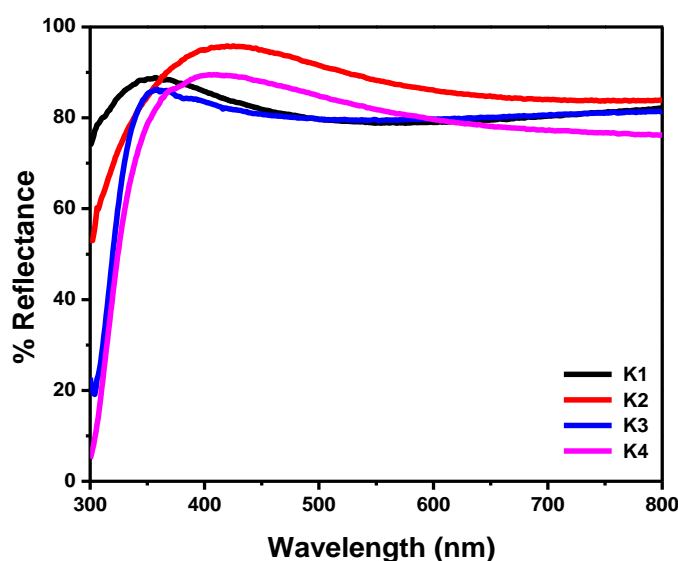


Figure 7. Reflectance spectra of 2%, 4%, 6% and 8% cobalt substituted SnO₂ thin films.

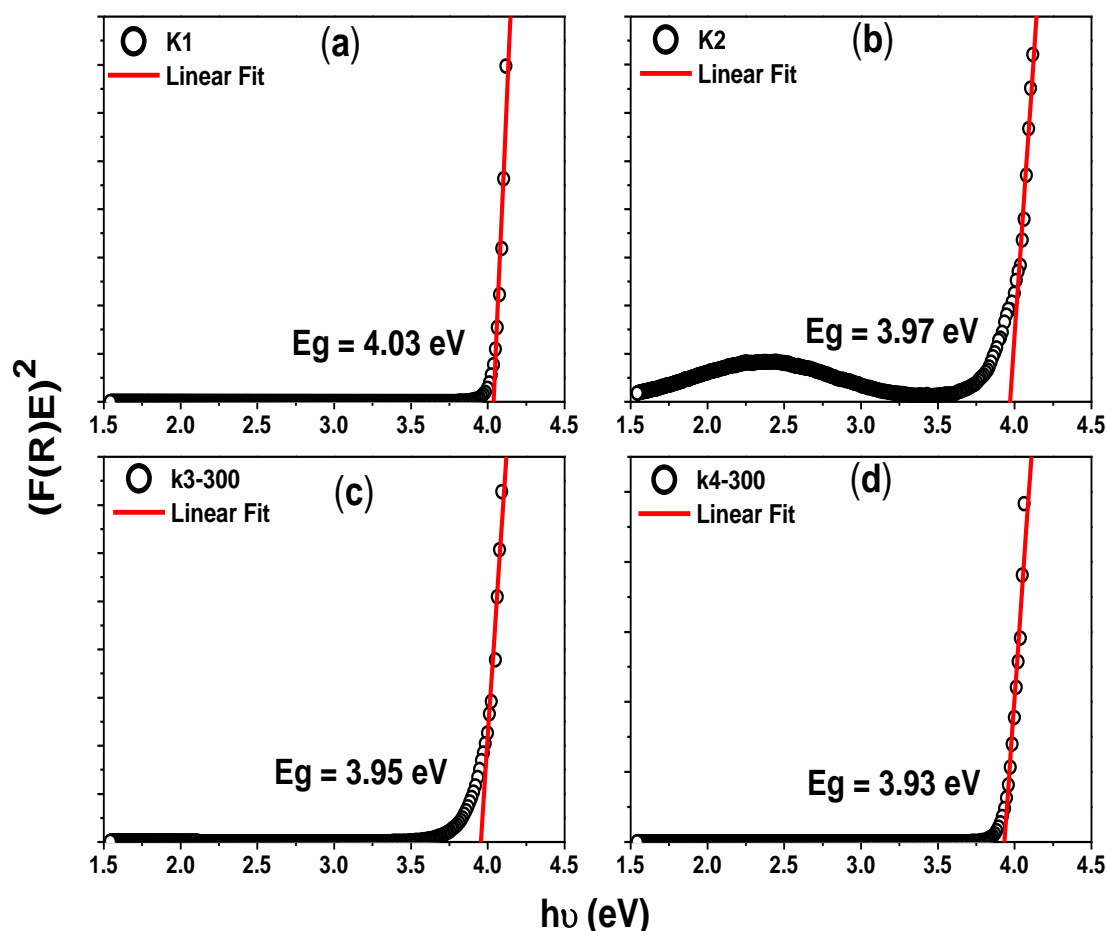


Figure 8. Modified Kubelka-Munk plot for 2%, 4%, 6%, and 8% cobalt substituted SnO₂ thin films.

Parameter S is a constant which is not related to wavelength. Hence $F(R)$ is directly proportional to the absorption coefficient. Then, the optical band gap was calculated using Tauc's equation: $F(R) \cdot h\nu = A (h\nu - E_g)^n$ Where A is a constant and the other parameters have their conventional meanings. The highest band gap value obtained for pure SnO₂ film and high reflectance is observed in the visible region as given in Figure 6 and the inset of Figure 6, respectively.

Figure 7 depicts the diffuse reflectance spectra of the prepared cobalt-substituted SnO₂ thin films. The prepared thin films are found to have maximum reflectance in the visible region of the spectrum. The modified Kubelka-Mulk plot of SnO₂ thin films is presented in Figure 8. The band gap energy can be determined by extrapolating the linear part to the energy axis. The calculated band gap values for undoped and Co substituted SnO₂ films were similar to the previous reports discussed earlier in Sec. 3.2. Significant decrease in bandgap from 4.04 eV to 3.93 eV with an increase in dopant concentration (Figure 8) is observed, which may be due to the shrinkage of the optical band gap.

3.2.2. Photoluminescence (PL) Spectra.

The PL spectra of the Co:SnO₂ thin films are shown in Figure 9. There is a broad emission spectrum centered around 460 nm with 420, 470, and 570 nm peaks. The 420, 470, and 570 nm peaks.

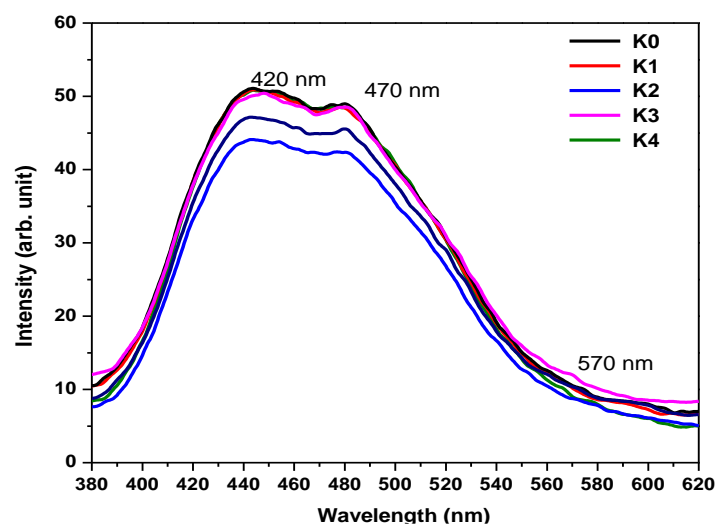


Figure 9. Photoluminescence spectra of undoped, 2 at%, 4 at%, 6 at%, and 8 at% Cobalt substituted SnO₂ thin films.

The emission band centered at 420 nm might have arisen from the intrinsic states localized on SnO₆ octahedra [65]. Similarly, the other two emissions, viz., the band centered at 470 nm, may be attributed to oxygen vacancy with doubly ionized oxygen vacancies and the band at 570 nm to the singly ionized oxygen vacancy. The intensity profiles suggest that the 2% Co-substituted SnO₂ thin films were found to have the lowest intensity. Such reduced intensity is a signature of slow down in the electron-hole pair recombination rate, which facilitates better photocatalytic performance [63].

3.3. Morphological properties.

The microstructures of the pristine and 2% Co-substituted SnO₂ thin films are shown in Figure 10. It illustrates that both SnO₂ and Co substituted films demonstrate spherical structure. It is evident that upon doping, a soft layer is covering the particles with improved particle size. It may be attributed to the role of cobalt on the nucleation and grain growth of SnO₂ thin films and improved crystallinity. These results are well accordance with the XRD results.

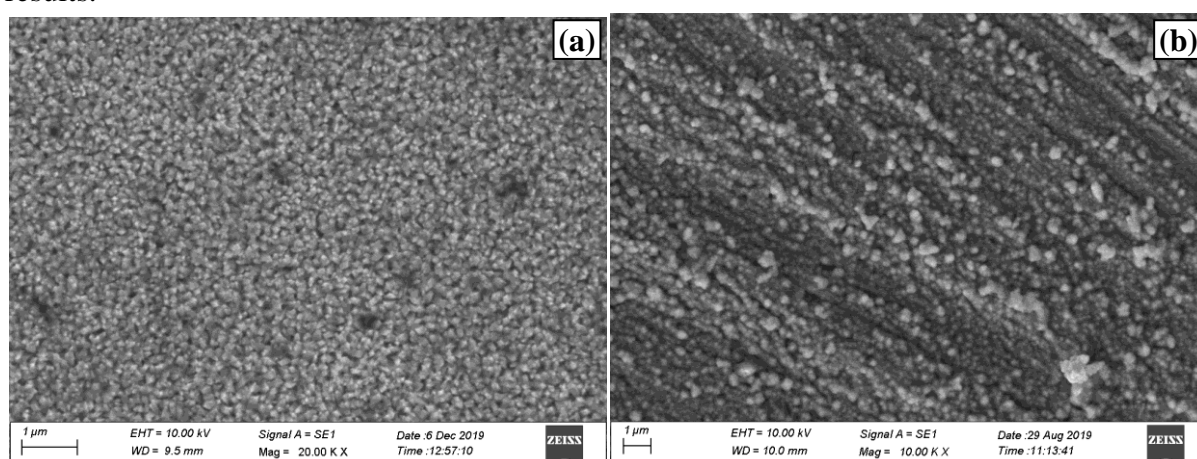


Figure 10. SEM micrographs of (a) undoped and (b) 2% Co-substituted SnO₂ thin films.

3.4. Photocatalytic activity.

Figure 11 (a) demonstrates the distinctions of absorption spectra of aqueous MB solution in the presence of the photo-catalysts-undoped SnO₂ thin films. The typical absorption

peak intensity of MB (664 nm) diminished adequately with the irradiation time through the dye-degradation process. The vanishing of the characteristic absorption peak of MB is traced, and it is represented in the Inset of Figure 10 (a). The undoped SnO₂ thin films exhibit 82.7% efficiency in 105 minutes. The trend of degradation efficiency, as given in Figure 10 (b), follows a nearly linear behavior within the time interval of measurement. The plot of $\ln(C/C_0)$ versus time enables one to calculate the rate constant, k (min⁻¹).

Figure 12 and 13 illustrate the degradation efficiency of cobalt-substituted SnO₂ thin films, and the efficiency and rate constant values hence estimated, are given in Table 2. The rate constant (k) and adj-R² values are estimated using the plots of $\ln(C/C_0)$ versus time (Figure 12). The effect of Co doping can be further elucidated clearly with the help of the dye-degradation efficiency plot shown in Figure 13. The proposed dye degradation mechanism of spray deposited Co-substituted SnO₂ thin films is illustrated in Figure 14.

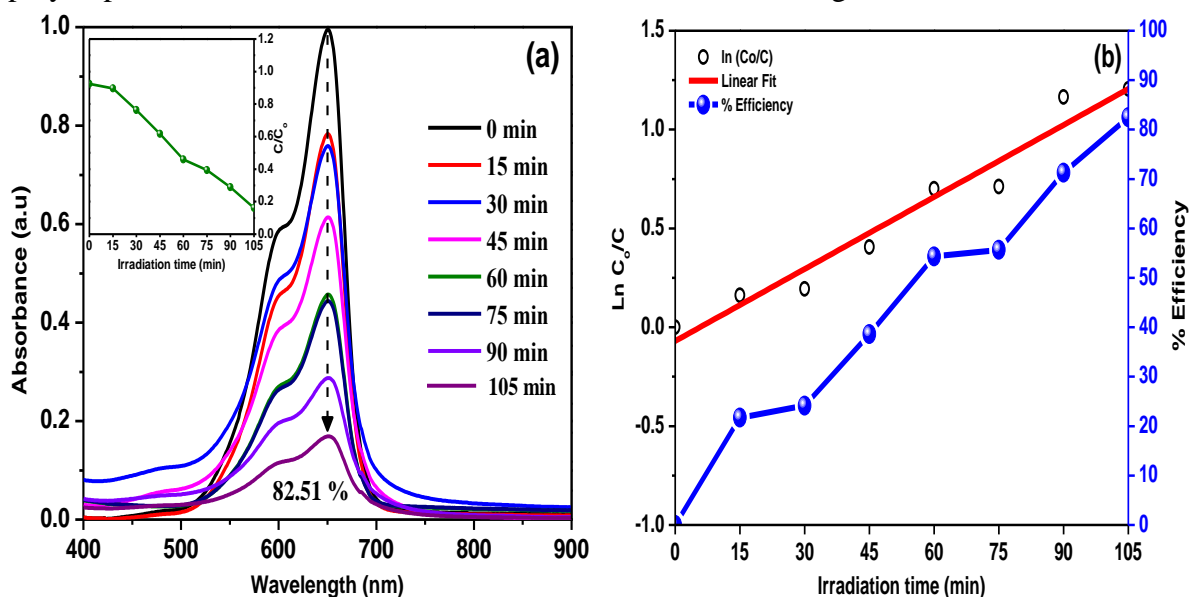


Figure 11.(a) Absorbance spectra of MB dye in the presence of pure SnO₂ thin films. Inset show Plot of (C/C_0) against time for pure SnO₂ thin films;(b) Plot of $\ln(C_0/C)$ against time for pure SnO₂ thin films.

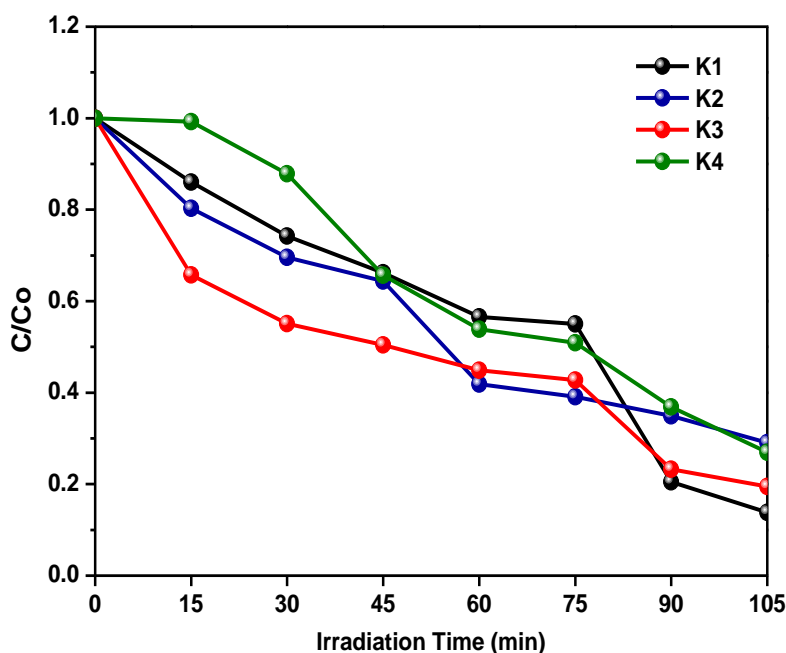


Figure 12. The plot of (C/C_0) against time for fabricated Co-substituted SnO₂ thin films.

Interestingly, the degradation efficiency depends on Co concentration and irradiation time, unlike the undoped SnO₂, which is reflected in the adj-R² values (Table 2). The deviation of adj-R² values in the present case indicates that cobalt doping enables a time-dependent degradation process. Thus, such degradation trends can suitably be harvested with the proper choice of concentration and irradiation time. However, Co:SnO₂ (2 at%) shows better photocatalytic activity among the investigated thin film samples.

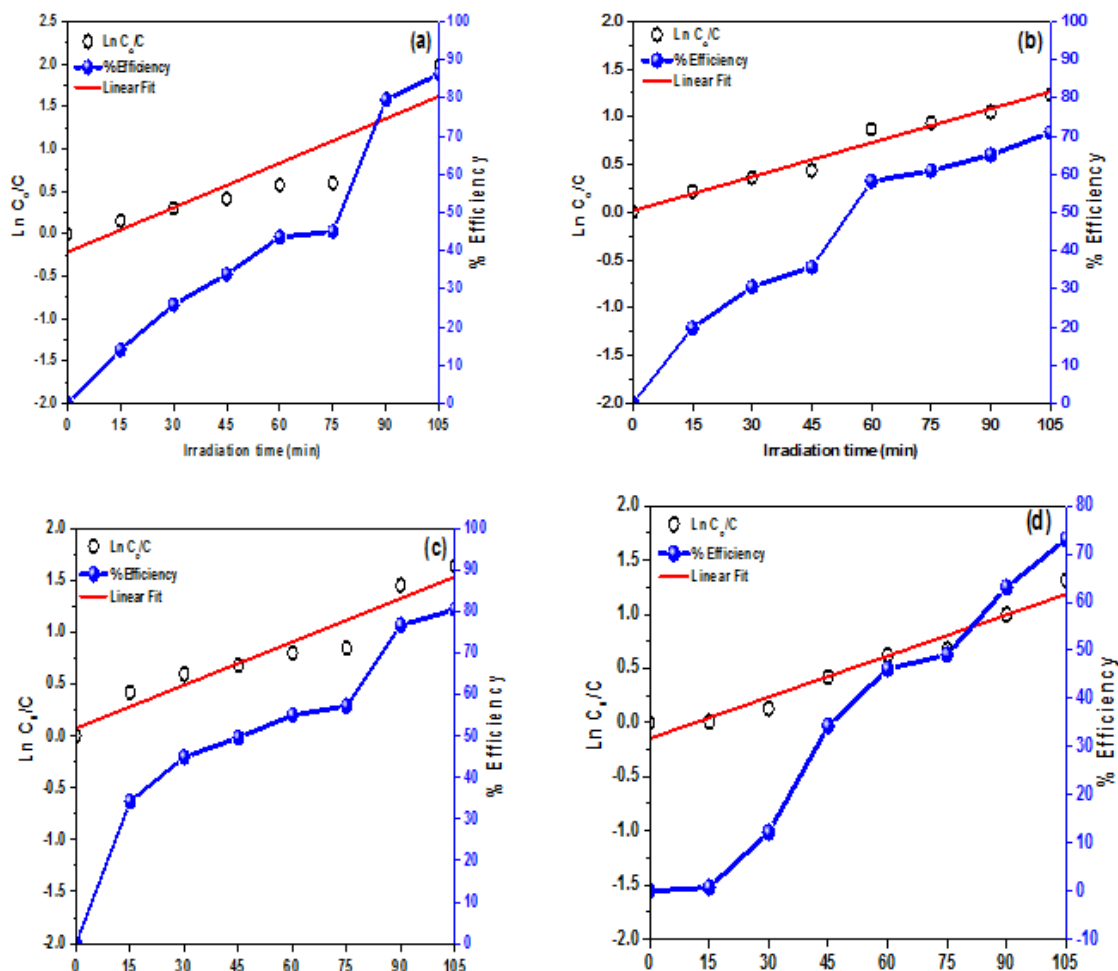


Figure 13. Plot of $\ln(C_0/C)$ against time for fabricated Co-substituted SnO₂ thin films.

Table 2. Degradation efficiency, regression coefficient (adj-R²), and rate constant (k) of the fabricated photocatalysts.

S.No.	Sample	Efficiency (%)	Adj-R ²	k (min ⁻¹)
1	K0	82.51	0.9508	0.01215
2	K1	86.19	0.8055	0.01753
3	K2	70.93	0.9692	0.01188
4	K3	80.55	0.9135	0.01391
5	K4	73.06	0.9510	0.01267

Table 3. Various reported photocatalytic activity of substituted SnO₂ photocatalysts.

S.No.	Photocatalyst	Light source	k (min ⁻¹)	Efficiency %	Degradation time (min)	Ref.
1	SnO ₂ :Co	UV- 150 W xenon lamp	0.01753	86	105	This work
2	SnO ₂	Philips TUV 8W	0.0073	96.8	280	[66]
3	ZnO	Philips TUV 8W	0.005	95	330	
4	PCz*	Lutron UV light meter UV-340A	0.00207	46.31	300	[67]
5	PCT1 ^s		0.00348	61.18	300	
6	PCT6 [#]		0.00282	95.67	300	
7	Ag/BWO	UV-A flexible	0.0044	81	420	[68]

S.No.	Photocatalyst	Light source	k (min ⁻¹)	Efficiency %	Degradation time (min)	Ref.
		LED strip (385 nm emission, 78 LEDs, 0.24 W/LED, total electric power~ 19 W, 13730 lux, and SMD 5050)				
8	0.2 art% Lu doped TiO ₂ thin films	11 W UV C lamp	0.009918	84	180	[69]
9	Iron Oxide NPs	high power LED visible light		72	90	[70]
10	MnTiO ₃ NPs	Five neck pyrex flask type reactor under sunlight irradiation	0.00525	70	240	[71]
11	MnTiO ₃ /TiO ₂ NPs	Five neck pyrex flask type reactor under sunlight irradiation	0.00596	75	240	

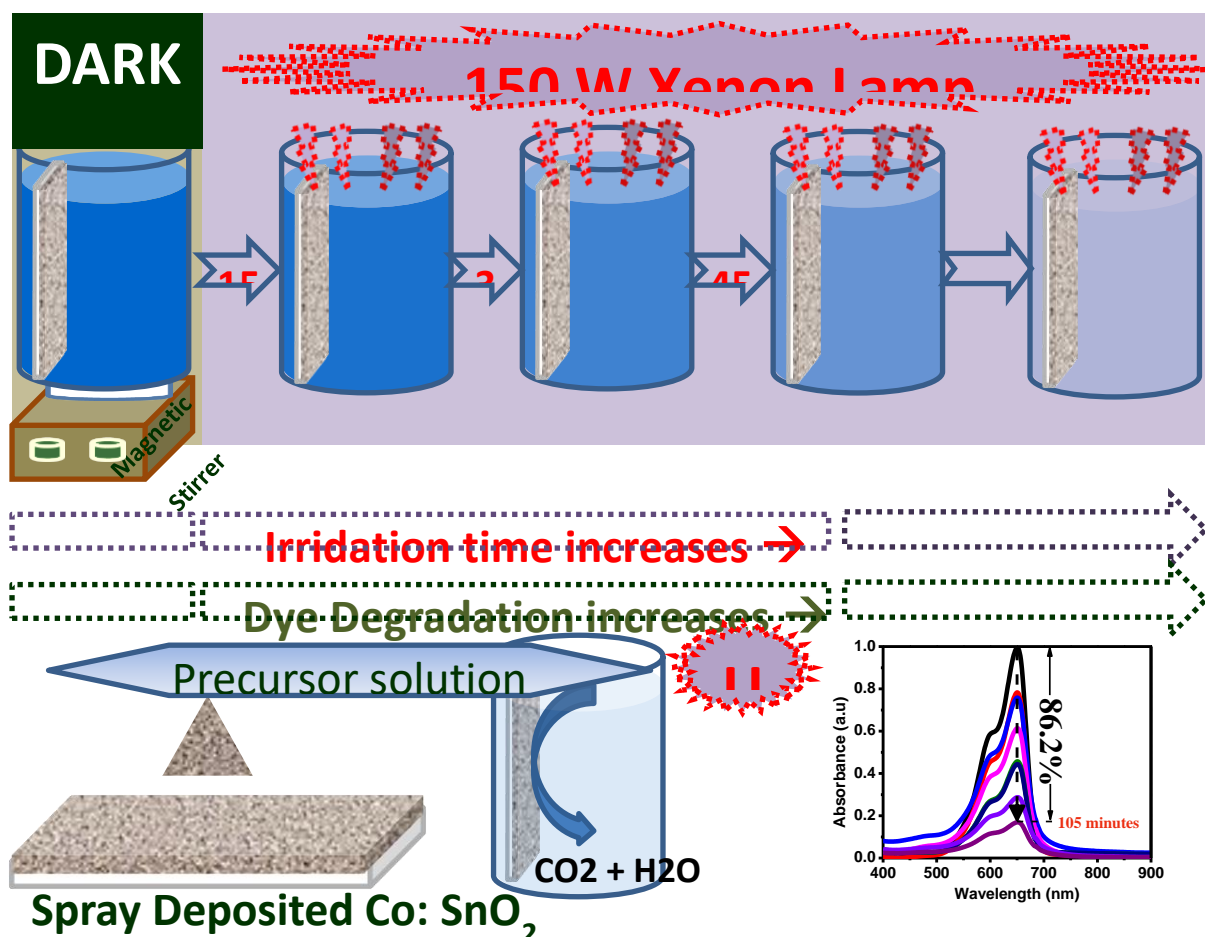


Figure 14. The proposed schematic of the M-B dye degradation mechanism by Co:SnO₂ thin films.

Thus, it can be inferred that the thin films formed with higher (4%, 6%, and 8%) doping concentrations have secondary phases of Sn₃O₄ which induce in the decrease of oxygen vacancies and facilitate the recombination of electrons and holes that diminish the photocatalytic efficiency. Table 3 gives the comparative literature with the values obtained from the present work.

4. Conclusions

Pure and Co-substituted SnO₂ nanoparticles deposited on the films are synthesized by spray pyrolysis. XRD studies reveal that the prepared thin films exhibit polycrystalline nature with a tetragonal rutile structure of SnO₂. The secondary phase corresponding to Sn₃O₄ is formed for higher cobalt concentrations, viz., 4%, 6%, and 8%. The crystallite size, as well as crystallinity, increases with cobalt concentration. Incorporating Co into the SnO₂ lattice results in red shifting of reflectance spectra and reduction in the optical band gap. The lowering of PL intensity hints at the delayed electron-hole pair recombination time. SEM images highlight that both pristine and Co-substituted SnO₂ films exhibit spherical structures. The photocatalytic activity towards Methylene dye is performed, and it is found that 2% Co–SnO₂ thin films show a better response. The improved photocatalytic performance of Co:SnO₂ thin films may be attributed to forming better and relaxed crystals and reducing recombination time. Studying the time-dependent degradation performance with varying cobalt concentrations is of further interest.

Funding

The authors declare that no funds, grants, or other support were received during the preparation of this manuscript.

Acknowledgments

Declared none.

Conflicts of Interest

The authors declare no conflict of interest.

References

1. Kansal, S.K.; Singh, M.; Sud, D. Studies on photodegradation of two commercial dyes in aqueous phase using different photocatalysts. *J. Hazard Mater.* **2007**, *141*, 581-590, <https://doi.org/10.1016/j.jhazmat.2006.07.035>.
2. Akpan, U.G.; Hameed, B.H. Parameters affecting the photocatalytic degradation of dyes using TiO₂-based photocatalysts: a review. *J. Hazard Mater.* **2009**, *170*, 520-529, <https://doi.org/10.1016/j.jhazmat.2009.05.039>.
3. Bhatkhande, D.S.; Pangarkar, V.G.; Beenackers, A.A. Photocatalytic degradation for environmental applications- a review. *J. Chem. Technol. Biotechnol.* **2002**, *77*, 102-116, <https://doi.org/10.1002/jctb.532>.
4. Wang, H.; Sun, F.; Zhang, Y.; Li, L.; Chen, H.; Wu, Q.; Yu, J.C. Photochemical growth of nanoporous SnO₂ at the air-water interface and its high photocatalytic activity. *J. Mater. Chem.* **2010**, *20*, 5641-5645, <https://doi.org/10.1039/B926930D>.
5. Fujishima, A.; Honda, K. Electrochemical photolysis of water at a semiconductor electrode. *Nature* **1972**, *238*, 37-38, <https://doi.org/10.1038/238037a0>.
6. Ohtani, B. Photocatalysis A to Z—what we know and what we do not know in a scientific sense. *J. Photochem. Photobiol. C* **2010**, *11*, 157-178, <https://doi.org/10.1016/j.jphotochemrev.2011.02.001>.
7. Herrmann, J.-M. Heterogeneous photocatalysis: fundamentals and applications to the removal of various types of aqueous pollutants. *Catal. Today* **1999**, *53*, 115-129, [https://doi.org/10.1016/S0920-5861\(99\)00107-8](https://doi.org/10.1016/S0920-5861(99)00107-8).
8. Niemeyer, C.M. Nanoparticles, Proteins, and Nucleic Acids: Biotechnology Meets Materials Science. *Angew. Chemie Int. Ed.* **2001**, *40*, 4128-4158, [https://doi.org/10.1002/1521-3773\(20011119\)40:22%3C4128::AID-ANIE4128%3E3.0.CO;2-S](https://doi.org/10.1002/1521-3773(20011119)40:22%3C4128::AID-ANIE4128%3E3.0.CO;2-S).

9. Katz, E.; Willner, I. Integrated Nanoparticle-Biomolecule Hybrid Systems: Synthesis, Properties, and Applications. *Angew. Chemie Int. Ed.* **2004**, *43*, 6042-6108, <https://doi.org/10.1002/anie.200400651>.
10. Agrawal, M.; Gupta, S.; Stamm, M. Recent developments in fabrication and applications of colloid based composite particles. *J. Mater. Chem.* **2011**, *21*, 615-627, <https://doi.org/10.1039/C0JM02631J>.
11. Aggarwal, P.; Hall, J.B.; McLeland, C.B.; Dobrovolskaia, M.A.; McNeil, S.E. Nanoparticle interaction with plasma proteins as it relates to particle biodistribution, biocompatibility and therapeutic efficacy. *Advanced Drug Delivery Reviews* **2009**, *61*, 428-437, <https://doi.org/10.1016/j.addr.2009.03.009>.
12. Grosse, P.; Schmitte, F.J.; Frank, G.; Köstlin, H. Preparation and growth of SnO₂ thin films and their optical and electrical properties. *Thin Solid Films* **1982**, *90*, 309-315, [https://doi.org/10.1016/0040-6090\(82\)90382-0](https://doi.org/10.1016/0040-6090(82)90382-0).
13. Tammina, S.K.; Mandal, B.K. Tyrosine mediated synthesis of SnO₂ nanoparticles and their photocatalytic activity towards Violet 4 BSN dye. *Journal of Molecular Liquids* **2016**, *221*, 415-421, <https://doi.org/10.1016/j.molliq.2016.05.079>.
14. Sadeghzadeh-Attar, A.; Bafandeh, M.R. The effect of annealing temperature on the structure and optical properties of well-aligned 1D SnO₂ nanowires synthesized using template-assisted deposition. *CrystEngComm* **2018**, *20*, 460-469, <https://doi.org/10.1039/C7CE01815K>.
15. Kumaravelan, S.; Seshadri, S.; Suresh, R.; Ravichandran, K.; Sathishkumar, P.; Shanthaseelan, K.; Suganthi, N. Effect of Zn dopant on SnO₂ nano-pyramids for photocatalytic degradation. *Chemical Physics Letters* **2021**, *769*, 138352, <https://doi.org/10.1016/j.cplett.2021.138352>.
16. Matussin, S.N.; Tan, A.L.; Harunsani, M.H.; Cho, M.H.; Khan, M.M. Green and Phytogenic Fabrication of Co-Doped SnO₂ Using Aqueous Leaf Extract of Tradescantia spathacea for Photoantioxidant and Photocatalytic Studies. *BioNanoScience* **2021**, *11*, 120-135, <https://doi.org/10.1007/s12668-020-00820-3>.
17. Soumya, S.S.; Xavier, T.S. Effect of cobalt doping on the microstructural, optical and electrical properties of SnO₂ thin films by sol-gel spin coating technique. *Physica B: Condensed Matter* **2022**, *624*, 413432, <https://doi.org/10.1016/j.physb.2021.413432>.
18. Chen, K.; Zhou, Y.; Jin, R.; Wang, T.; Liu, F.; Wang, C.; Yan, X.; Sun, P.; Lu, G. Gas sensor based on cobalt-doped 3D inverse opal SnO₂ for air quality monitoring. *Sensors and Actuators B: Chemical* **2022**, *350*, 130807, <https://doi.org/10.1016/j.snb.2021.130807>.
19. Pazouki, S.; Memarian, N. Effects of Hydrothermal temperature on the physical properties and anomalous band gap behavior of ultrafine SnO₂ nanoparticles. *Optik* **2021**, *246*, 167843, <https://doi.org/10.1016/j.ijleo.2021.167843>.
20. Chang, Y.-C.; Wu, S.-H. Bi-functional Al-doped ZnO@SnO₂ heteronanowires as efficient substrates for improving photocatalytic and SERS performance. *Journal of Industrial and Engineering Chemistry* **2019**, *76*, 333-343, <https://doi.org/10.1016/j.jiec.2019.03.058>.
21. Soltan, W.B.; Ammar, S.; Olivier, C.; Toupance, T. Influence of zinc doping on the photocatalytic activity of nanocrystalline SnO₂ particles synthesized by the polyol method for enhanced degradation of organic dyes. *Journal of Alloys and Compounds* **2017**, *729*, 638-647, <https://doi.org/10.1016/j.jallcom.2017.09.155>.
22. Huang, R.; Huang, S.; Chen, D.; Zhang, Q.; Le, T.-T.; Wang, Q.; Hu, Z.; Chen, Z. Environmentally benign synthesis of Co₃O₄-SnO₂ heteronanorods with efficient photocatalytic performance activated by visible light. *Journal of Colloid and Interface Science* **2019**, *542*, 460-468, <https://doi.org/10.1016/j.jcis.2019.01.089>.
23. Yakout, S.M. Robust ferromagnetic and fast sunlight photocatalytic properties of nanocrystalline SnO₂: Co/Cu codoping. *Ceramics International* **2021**, *47*, 10104-10112, <https://doi.org/10.1016/j.ceramint.2020.12.158>.
24. Toloman, D.; Popa, A.; Stefan, M.; Silipas, T.D.; Suciu, R.C.; Barbu-Tudoran, L.; Pana, O. Enhanced photocatalytic activity of Co doped SnO₂ nanoparticles by controlling the oxygen vacancy states. *Optical Materials* **2020**, *110*, 110472, <https://doi.org/10.1016/j.optmat.2020.110472>.
25. Khan, D.; Rehman, A.; Rafiq, M.Z.; Khan, A.M.; Ali, M. Improving the optical properties of SnO₂ nanoparticles through Ni doping by sol-gel technique. *Current Research in Green and Sustainable Chemistry* **2021**, *4*, 100079, <https://doi.org/10.1016/j.crgsc.2021.100079>.
26. Alborno, L.L.; da Silva, S.W.; Bortolozzi, J.P.; Banús, E.D.; Brussino, P.; Ulla, M.A.; Bernardes, A.M. Degradation and mineralization of erythromycin by heterogeneous photocatalysis using SnO₂-doped TiO₂ structured catalysts: Activity and stability. *Chemosphere* **2021**, *268*, 128858, <https://doi.org/10.1016/j.chemosphere.2020.128858>.

27. Lin, B.; Xu, B.; Zhou, Y.; Zhu, B.; Chen, Y.; Gao, B. Heterostructured SnO₂-pillared Co-doped tantalotungstate with high photocatalytic activity under visible-light irradiation. *Materials Chemistry and Physics* **2013**, *142*, 651–658, <https://doi.org/10.1016/j.matchemphys.2013.08.015>.
28. Al-Hamdi, A.M.; Rinner, U.; Sillanpää, M. Tin dioxide as a photocatalyst for water treatment: A review. *Process Safety and Environmental Protection* **2017**, *107*, 190–205, <https://doi.org/10.1016/j.psep.2017.01.022>.
29. Sery, A.A.; Mohamed, W.A.A.; Hammad, F.F.; Khalil, M.M.H.; Farag, H.K. Synthesis of pure and doped SnO₂ and NiO nanoparticles and evaluation of their photocatalytic activity. *Materials Chemistry and Physics* **2022**, *275*, 125190, <https://doi.org/10.1016/j.matchemphys.2021.125190>.
30. Bannur, M.S.; Antony, A.; Maddani, K.I.; Poornesh, P.; Manjunatha, K.B.; Kulkarni, S.D.; Choudhari, K.S. Role of Ba in engineering band gap, photoluminescence and nonlinear optical properties of SnO₂ nanostructures for photovoltaic and photocatalytic applications. *Superlattices and Microstructures* **2018**, *122*, 156–164, <https://doi.org/10.1016/j.spmi.2018.08.012>.
31. Sarangi, S.N.; Pradhan, G.K.; Samal, D. Band gap engineering in SnO₂ by Pb doping. *Journal of Alloys and Compounds* **2018**, *762*, 16–20, <https://doi.org/10.1016/j.jallcom.2018.05.143>.
32. Chetri, P.; Dhar, J.C. Modification of defects in SnO₂ nanowire arrays by gallium doping for enhanced photodetection. *Journal of Alloys and Compounds* **2022**, *899*, 163402, <https://doi.org/10.1016/j.jallcom.2021.163402>.
33. Jasim, K.E.; Dakhel, A.A. Role of (Cu, Al) codoping in tuning the optical, structural and magnetic properties of Co-doped SnO₂ nanostructures: A comparative study. *Physica B: Condensed Matter* **2021**, *614*, 413040, <https://doi.org/10.1016/j.physb.2021.413040>.
34. Entradas, T.; Cabrita, J.F.; Dalui, S.; Nunes, M.R.; Monteiro, O.C.; Silvestre, A.J. Synthesis of sub-5 nm Co-doped SnO₂ nanoparticles and their structural, microstructural, optical and photocatalytic properties. *Materials Chemistry and Physics* **2014**, *147*, 563–571, <https://doi.org/10.1016/j.matchemphys.2014.05.032>.
35. Afify, N.; Abbady, G.; Hamad, D.; Abdelbaki, R.F.; Yousef, E.S.; Shaaban, E.R.; N. Abd-el Salam, M. The effective role of dilute Co on SnO₂ nanoparticles: Structural, optical and magnetic characterization properties for spintronics. *Sensors and Actuators A: Physical* **2021**, *331*, 112984, <https://doi.org/10.1016/j.sna.2021.112984>.
36. Mazloom, J.; Ghodsi, F.E. Spectroscopic, microscopic, and electrical characterization of nanostructured SnO₂:Co thin films prepared by sol–gel spin coating technique. *Materials Research Bulletin* **2013**, *48*, 1468–1476, <https://doi.org/10.1016/j.materresbull.2012.12.069>.
37. Puga, F.; Navío, J.A.; Hidalgo, M.C. Enhanced UV and visible light photocatalytic properties of synthesized AgBr/SnO₂ composites. *Separation and Purification Technology* **2021**, *257*, 117948, <https://doi.org/10.1016/j.seppur.2020.117948>.
38. Mendoza-Damián, G.; Tzompantzi, F.; Pérez-Hernández, R.; Gómez, R.; Hernández-Gordillo, A. Photocatalytic properties of boehmite–SnO₂ composites for the degradation of phenol. *Catalysis Today* **2016**, *266*, 82–89, <https://doi.org/10.1016/j.cattod.2015.11.029>.
39. Gürakar, S.; Serin, T. Effect of Co doping on optical parameters of SnO₂ thin films. *Optical Materials* **2021**, *111*, 110579, <https://doi.org/10.1016/j.optmat.2020.110579>.
40. Rajan, R.; Vizhi, R.E. Effect of Co³⁺ substitution on the structural, optical, and room-temperature magnetic properties of SnO₂ nanoparticulates. *Journal of Materials Science: Materials in Electronics* **2021**, *32*, 12716–12724, <https://doi.org/10.1007/s10854-021-05906-6>.
41. Peng, Z.; Shi, Z.; Liu, M. Mesoporous Sn–TiO₂ composite electrodes for lithium batteries. *Chem. Commun.* **2000**, *21*, 2125–2126, <https://doi.org/10.1039/B007687M>.
42. Ferrere, S.; Zaban, A.; Gregg, B.A. Dye Sensitization of Nanocrystalline Tin Oxide by Perylene Derivatives. *J. Phys. Chem. B* **1997**, *101*, 4490–4493, <https://doi.org/10.1021/jp970683d>.
43. He, Y.S.; Campbell, J.C.; Murphy, R.C.; Arendt, M.F.; Swinnea, J.S. Electrical and optical characterization of Sb:SnO₂. *J. Mater. Res.* **2011**, *8*, 3131–3134, <https://doi.org/10.1557/JMR.1993.3131>.
44. Seal, S.; Shukla, S. Nanocrystalline SnO gas sensors in view of surface reactions and modifications. *JOM* **2002**, *54*, 35–38, <https://doi.org/10.1007/BF02709091>.
45. Chopra, K.L.; Major, S.; Pandya, D.K. Transparent conductors—A status review. *Thin Solid Films* **1983**, *102*, 1–46, [https://doi.org/10.1016/0040-6090\(83\)90256-0](https://doi.org/10.1016/0040-6090(83)90256-0).
46. Fang, L.M.; Zu, X.T.; Li, Z.J. et. al. Microstructure and luminescence properties of Co-doped SnO₂ nanoparticles synthesized by hydrothermal method. *J. Mater. Sci. Mater. Electron* **2008**, *19*, 868–874, <https://doi.org/10.1007/s10854-007-9543-7>.

47. Zinatloo-Ajabshir, S.; Salavati-Niasari, M. Synthesis, characterization, optical and photocatalytic properties Nanocrystalline Pr_6O_{11} . *New J. Chem* **2015**, *39*, 3948–3955, <https://doi.org/10.1039/C4NJ02106A>.
48. Salavati-Niasari, M.; Mir, N.; Davar, F. Synthesis, characterization and optical properties of tin oxide nanoclusters prepared from a novel precursor via thermal decomposition route. *Inorganica Chim. Acta* **2010**, *363*, 1719–1726, <https://doi.org/10.1016/j.ica.2010.03.024>.
49. Zhou, J.G.; Fang, H.T.; J.M.et. al. An X-ray Absorption, Photoemission, and Raman Study of the Interaction between SnO_2 Nanoparticle and Carbon Nanotube. *J. Phys. Chem. C* **2009**, *113*, 6114–6117, <https://doi.org/10.1021/jp013214r>.
50. Dai, Z.R.; Gole, J.L.; Stout, J.D.; Wang, Z.L. Tin Oxide Nanowires, Nanoribbons, and Nanotubes. *J. Phys. Chem. B* **2002**, *106* 1274–1279, <https://doi.org/10.1021/jp013214r>.
51. Wu, P.; Du, N.; Zhang, H.; Zhai, C.; Yang, D. Self-Templating Synthesis of SnO_2 - Carbon Hybrid Hollow Spheres for Superior Reversible Lithium Ion Storage. *ACS Appl. Mater. Interfaces* **2011**, *3*, 1946–1952, <https://doi.org/10.1021/am200168w>.
52. Xing, J.; Fang, W.Q.; Li, Z.; Yang, H.G. TiO_2 -Coated Ultrathin SnO_2 Nanosheets Used as Photoanodes for Dye-Sensitized Solar Cells with High Efficiency. *Ind. Eng. Chem. Res.* **2012**, *51*, 4247–4253, <https://doi.org/10.1021/ie2030823>.
53. Sinha, A.K.; Pradhan, M.; Sarkar, S.; Pal, T. Large-Scale Solid-State Synthesis of Sn-SnO_2 Nanoparticles from Layered SnO by Sunlight: a Material for Dye Degradation in Water by Photocatalytic Reaction. *Environ. Sci. Technol* **2013**, *47*, 2339–2345, <https://doi.org/10.1021/es303413q>.
54. Morassaei, M.S.; Zinatloo-Ajabshir, S.; Salavati-Niasari, M. New facile synthesis, structural and photocatalytic studies of $\text{NdOCl-Nd}_2\text{Sn}_2\text{O}_7\text{-SnO}_2$ nanocomposites. *J. Mol. Liq.* **2016**, *220*, 902–909, <https://doi.org/10.1016/j.molliq.2016.05.041>.
55. Nilavazhagan, S.; Muthukumaran, S.; Ashokkumar, M. Structural, optical and morphological properties of La, Cu co-doped SnO_2 nanocrystals by co-precipitation method. *Opt. Mater* **2014**, *37*, 425, <https://doi.org/10.1016/j.optmat.2014.07.003>.
56. Zima, T.; Bulina, N. Enhanced room-temperature ferromagnetism of Co-doped SnO_2 nanostructures produced by the hydrothermal method. *Mater. Res. Bull* **2019**, *117*, 48–55, <https://doi.org/10.1016/j.materresbull.2019.04.018>.
57. Srinatha, N.; No, Y.S.; Kamble, V.B.; Chakravarty, S.; Suriyamurthy, N.; Angadi, B.; Umarji, A.M.; Choi, W.K. Effect of RF power on the structural, optical and gas sensing properties of RF-sputtered Al doped ZnO thin films. *RSC Adv* **2016**, *6*, 9779–9788, <https://doi.org/10.1039/C5RA22795J>.
58. Sadeghzadeh-Attar, A.; Bafandeh, M.R. The effect of annealing temperature on the structure and optical properties of well-aligned 1D SnO_2 nanowires synthesized using template-assisted deposition. *CrystEngComm* **2018**, *20*, 460–469, <https://doi.org/10.1039/C7CE01815K>.
59. Reddy, K.S.; Nithiyanantham, S.; Geetha, G.; Sujatha, R.A.; Mahalakshmi, S. Study of structural and optical properties of Fe^{2+} doped tin oxide nanoparticles. *J. Mater. Appl.* **2019**, *8*, 8–12, <https://doi.org/10.32732/jma.2019.8.1.8>.
60. Singh, M.; Goyal, M.; Devlal, K. Size and Shape Effects on the Band Gap of Semiconductor Compound Nanomaterials. *Journal of Taibah University for Science* **2018**, *12*, 470–475, <https://doi.org/10.1080/16583655.2018.1473946>.
61. Bouaine, A.; Brihi, N.; Schmerber, G.; Ulhaq-Bouillet, C.; Colis, S.; Dinia, A. Structural, optical, and magnetic properties of Co-doped SnO_2 powders synthesized by the coprecipitation technique. *J. Phys. Chem. C* **2007**, *111*, 2924–2928, <https://doi.org/10.1021/jp066897p>.
62. Antony, A.; Bannur, M.S.; Antony, A.; Maddani, K.I.; Poornesh, P.; Rao, A.; Choudhari, K.S. Tailoring the nonlinear optical susceptibility $\chi(3)$ photoluminescence and optical band gap of nanostructured SnO thin films by Zn doping for photonic device applications. *Phys. E: Low-Dimensional Syst. Nanostructures* **2018**, *103*, 348–353, <https://doi.org/10.1016/j.physe.2018.06.025>.
63. Kim, C.H.; Kim, B.H.; Yang, K.S. TiO_2 nanoparticles loaded on graphene/carbon composite nanofibers by electrospinning for increased photocatalysis. *Carbon* **2012**, *50*, 2472–2481, <https://doi.org/10.1016/j.carbon.2012.01.069>.
64. Mohammed Gazzali, P.M.; Rajan, S.; Chandrasekaran, G. Transformation from conducting ferromagnetic to insulating diamagnetic in vanadium doped ZnO nanoparticles. *Journal of Materials Science: Materials in Electronics* **2018**, *29*, 823–836, <https://doi.org/10.1007/s10854-017-7977-0>.

65. Lei, Y.; Zhang, L.D.; Meng, G.W.; Li, G.H.; Zhang, X.Y.; Liang, C.H.; Chen, W.; Wang, S.X. Preparation and photoluminescence of highly ordered TiO₂ nanowire arrays. *Appl. Phys. Lett.* **2001**, *78*, 1125–1127, <https://doi.org/10.1063/1.1350959>.
66. Chanu, L.A.; Singh, K.J.; Devi, K.N. Study on the Photocatalytic Activity of Metal Oxide Nanoparticles towards the Degradation of Some Organic Dyes. *Integrated Ferroelectrics* **2020**, *204*, 90-99, <https://doi.org/10.1080/10584587.2019.1674977>.
67. Ali, M.M.; Williams, D.J.; Banu, M.S. Enhanced photocatalytic activity of annealed polycarbazole-tin oxide nanocomposite against RhB and MB dyes under UV and natural sunlight irradiations. *Journal of Polymer Research* **2020**, *27*, 338, <https://doi.org/10.1007/s10965-020-02165-7>.
68. Segovia-Sandoval, S.J.; Ojeda-Galván, H.J.; Moral-Rodríguez, A.I.; Rodríguez-Hernández, J.; Peralta-Rodríguez, R.D.; Gómez-Villegas, K.J.; Hernández-Juárez, N.I.; Mendoza-Mendoza, E. A novel green synthesis of Bi₂WO₆-based photocatalysts for efficient pollutants degradation using low-power UV-A LEDs. *Journal of Alloys and Compounds* **2022**, *911*, 165018, <https://doi.org/10.1016/j.jallcom.2022.165018>.
69. Kompa, A.; Kekuda, D.; Murari, M.S.; Mohan Rao, K. Defect induced enhanced catalytic activity of Lu doped titanium dioxide (TiO₂) thin films. *Surfaces and Interfaces* **2022**, *31*, 101988, <https://doi.org/10.1016/j.surfin.2022.101988>.
70. Hirad, A.H.; Ansari, S.A.; Ali, M.A.E.; Egeh, M.A. Microwave-mediated synthesis of iron oxide nanoparticles: Photocatalytic, antimicrobial and their cytotoxicity assessment. *Process Biochemistry* **2022**, *118*, 205-214, <https://doi.org/10.1016/j.procbio.2022.04.022>.
71. Alkaykh, S.; Mbarek, A.; Ali-Shattle, E.E. Photocatalytic degradation of methylene blue dye in aqueous solution by MnTiO₃ nanoparticles under sunlight irradiation. *Heliyon* **2020**, *6*, e03663, <https://doi.org/10.1016/j.heliyon.2020.e03663>.